J. Photochem. Photobiol. A: Chem., 82 (1994) 87–101

Electron transfer rates from time-dependent correlation functions. Wavepacket dynamics, solvent effects, and applications

Matthew D. Todd[†], Abraham Nitzan[††], Mark A. Ratner[†††] and Joseph T. Hupp
Department of Chemistry and Materials Research Center, Northwestern University, Evanston, IL 60208 (USA)

Abstract

The golden-rule expression for the non-adiabatic electron-transfer rate constant in donor/acceptor systems is analyzed using a Fourier (time-dependent) representation. The rate constant is written in terms of an evolving overlap of wavepackets on initial and final state potential-energy surfaces. By following the explicit time-dependence of these functions, we can obtain both standard results of electron-transfer theory for the specific case of a standard polaron-type model (including inverted-region behavior, temperature dependence, nuclear tunneling effects, energy sharing) and some important generalizations, including situations of breakdown of the Condon approximation, analysis of the effects of frequency changes, and simplifications of the relevant vibrational modes due to solvent, to intra-molecular vibrations, or to both.

The correlation-function method is briefly described, and results of a number of calculations are discussed. Analysis includes the effects of inhomogeneous broadening and of energy flow into solvent and vibrational degrees of freedom. Analysis of two particular cases, subjects of recent elegant experimental investigation, are included to show the applicability of the technique.

1. Introduction

Present theoretical models for the elucidation of electron transfer (ET) in molecular systems trace their origins back to the early work of Marcus [1] and Hush [2], in which they proposed a transition-state theory model for electron transfer. Later models made use of a small-polaron approach, in which harmonic surfaces were defined with linear electronic–vibrational coupling [3–6][§,§§]; these permit treatment of low-temperature rates associated with nuclear and electronic tunneling.

We have recently presented a new approach to ET rate theory based on an explicitly time-dependent reformulation of superexchange-assisted non-adiabatic ET [12]. Here, we present the two-site version of this approach. It is essentially a polaron model, in which electronic and nuclear motion are linearly coupled, but it allows for an explicitly time-dependent computation of the electron-transfer process, offering dynamic as well as energetic information. This analysis therefore represents a generalization of Marcus–Hush theory. Initial- and final-state electronic surfaces may be harmonic or anharmonic, and the equations of motion allow for frequency changes. The model can include temperature variation, anharmonicity, breakdown of the Condon approximation, and solvent dynamical and energetic effects, making it possible to observe directly how these affect the non-adiabatic electron-transfer process. Furthermore, the model can be extended to a superexchange picture which explicitly includes bridge dynamics [12].

Recent resonance or near-resonance Raman studies on charge-transfer systems by the groups of Gould and Myers [13] and Hupp and Barbara [14] have provided direct measurements of vibrational frequencies and displacements, which in turn define the appropriate parameters used in our model [12]. Here, we present a numerical analysis of the two-site non-adiabatic ET model, applied to a model system as well as the experimentally studied ET systems, and discuss it in terms of solvent, temperature, frequency change,

[†]Present address: Department of Chemistry, Aarhus University, Langelandsgade 140, DK-8000 Århus C, Denmark.

[††]Permanent address: School of Chemistry, Sackler Faculty of Science, Tel Aviv University, Tel Aviv 69978, Israel.

[†††]Author to whom correspondence should be addressed.

[§]For recent reviews see, for example, ref. 7.

[§§]Also see ref. 8. Correlation-function approaches to the rate constant have been used extensively; see, for example, ref. 9. See also ref. 10 and Chaps. 7–10 of ref. 11.

SSDI 1010-6030(94)02017-H

and coupling effects. Finally, we compare it to the related, but distinct, polaron treatment of Fischer and van Duyne [8].

2. The model

The two-site model is essentially a linearly-coupled displaced oscillator system [7,12]. It has been used to describe non-adiabatic electron transfer between two states defined by electronic surfaces I and F, which in turn consist of vibronic levels i and f, respectively. At its simplest level (harmonic surfaces, linear displacement coupling, Condon approximation, etc.), the model is essentially the standard polaron treatment [4–8], but the analysis may be easily extended to include anharmonicity, solvent effects, breakdown of the Condon approximation, etc. In addition, the treatment of the model differs substantially from that of the usual polaron system, allowing for a *dynamic* rather than *energetic* view of the electron-transfer process.

Figure 1 shows a one-dimensional depiction of the simplest model, including two harmonic surfaces (initial- and final-state electronic surfaces, with minima at X_I^0 and X_F^0, respectively), their energetic and nuclear coordinate displacements (ΔE and $(X_F^0 - X_I^0)$, respectively), and the total reorganization energy λ. The ET rate then corresponds to motion of the system from the bottom of the left well to that of the right well.

After rewriting the golden-rule rate expression in dynamical form and separating the model hamiltonian into nuclear and electronic parts, the rate of transition from state I to state F in the two-site case is given by [12]

$$\Gamma_I = |V_{IF}|^2 \int_0^\infty dt\, e^{-i\Delta E t} \langle i | e^{iH_F t}\, e^{-iH_I t} | i \rangle_T \qquad (1)$$

in which V_{IF} is the electronic coupling matrix element between states I and F, ΔE is the difference in energy between states I and F, H_s is the nuclear hamiltonian for state s (=I,F), and $\langle ... \rangle_T$ refers to a thermal average over initial and final vibronic states. Here we have also assumed the Condon approximation, so that $V_{if} = V_{IF}$ for all i and f, and $\hbar \equiv 1$.

Calculation of rates then involves propagation of initial and final state wavepackets, evolving according to H_I and H_F, respectively, and analyzing the thermal average in eqn. (1), followed by a time integral. Anharmonicities and frequency changes are included in H_s (Section 9), temperature effects are included in the thermal average over a Boltzmann distribution of initial states (Section 8), and effects of the breakdown of the Condon approximation can be included by making V time-dependent, and including it in the time integral. Observation of the integrand of eqn. (1) allows a detailed, time-dependent, dynamical analysis of the electron transfer process (see, for example, Figs. 2–5).

3. Semi-classical treatment and gaussian wavepackets

Following Neria *et al.* [15], we now make a semi-classical approximation by replacing $|i\rangle$ in eqn. (1)

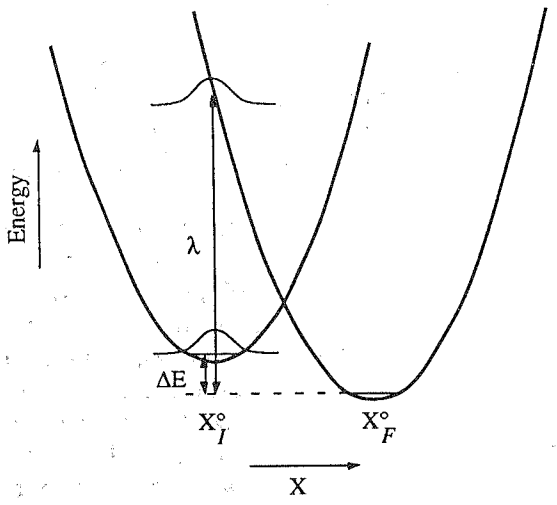

Fig. 1. A model one-dimensional, two-site, non-adiabatic system, with reorganization energy λ and energy difference ΔE.

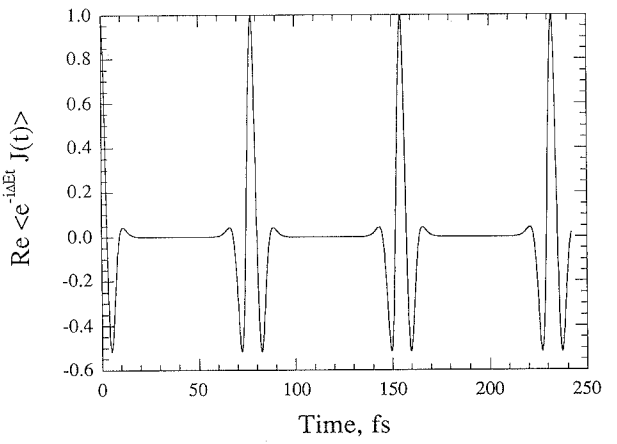

Fig. 2. $\exp[-i\Delta E t]J(t)$ for the model Fe (2+/3+) system described in the text and Table 1. $J(t)$ here is as defined in eqn. (4b), and thus, in this and subsequent figures, the vertical axis is unitless. Relevant parameters for the one-mode case shown are as follows: $\hbar\omega = 431$ cm^{-1}; $\lambda_i = 2926$ cm^{-1}; $\Delta E_{IF} = 0$; $T = 0$ K. Note that, in the absence of irreversible processes, we observe recurrences.

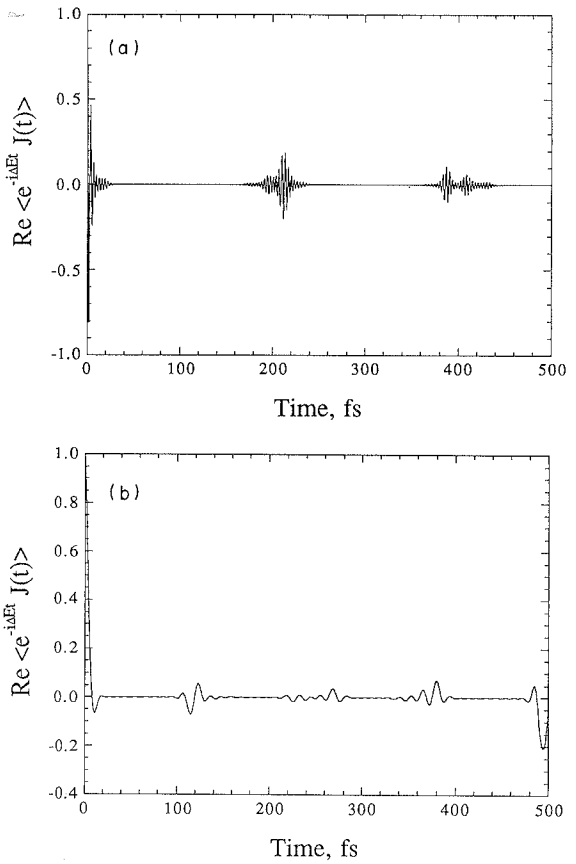

Fig. 3. $\exp(-i\Delta Et)J(t)$ for (a) the HMB/TCNE ($\Delta E_{IF}=11\ 600$ cm^{-1}; $V_{IF}\approx 3500$ cm^{-1}; $\lambda_i=3515$ cm^{-1}) and (b) the Ru/Fe charge transfer systems ($\Delta E_{IF}=3000$ cm^{-1}; $V_{IF}\approx 3200$ cm^{-1}; $\lambda_i=3220$ cm^{-1}) (see text). These are single trajectories, with $T=0$ K.

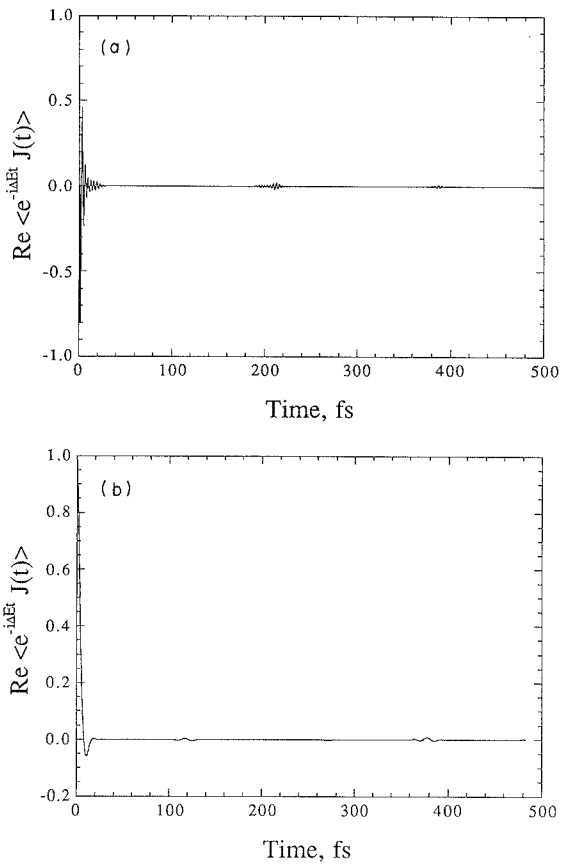

Fig. 4. $\langle\exp[-i\Delta Et]J(t)\rangle$ for (a) the HMB/TCNE and (b) the Ru/Fe charge transfer systems, with 200 cm^{-1} of inhomogeneous electronic gap modulation added (see text and Fig. 3). These represent the average of 200 trajectories (sufficient to give convergence of $C(t)$), with trajectories chosen at $T=0$ K.

by gaussian wavepackets centered about the classical position and momenta of the atomic nuclei moving on the I potential surface. Gaussian wavepackets are sketched in Fig. 1 (shown at $t=0$ with zero momentum). They are propagated using the nuclear hamiltonians [16]

$$H_s=-\frac{1}{2m}\frac{\partial^2}{\partial X^2}+V_s(X) \tag{2}$$

on the electronic surfaces S = I and F, defined by $V_S(X)$; here, m is the reduced mass, and $\hbar\equiv 1$ [16]. The thermal average is implemented by sampling the classical positions and momenta on surface I from a Boltzmann distribution.

Equation (1) then leads to

$$\Gamma_I=\int_{-\infty}^{+\infty} dt\ e^{-i\Delta Et}C(t) \tag{3}$$

where

$$C(t)\equiv|V_{IF}|^2\langle J(t)\rangle_T \tag{4a}$$

and

$$J(t)=\langle i(0)|e^{iH_Ft}\ e^{-iH_It}|i(0)\rangle \tag{4b}$$

Here, $C(t)$ contains a thermal average over nuclear potential energies and wavefunction overlaps ($\langle\ldots\rangle_T$). The correlation function $J(t)$ represents the overlap, at time t, between the two wavepackets which start as $i(0)$ at $t=0$; one wavepacket is propagated on surface I, while the other is propagated on surface F. $J(t)$ is thus essentially a time-dependent Franck–Condon amplitude.

Neria *et al.* [15] have used the frozen gaussian approximation (FGA) of Heller [16(b)] to implement the time evolutions in eqn. (4b); however, this is not necessary (although justified in many condensed-phase processes, owing to the short relaxation time of this function). The general approach of Heller [16(b)] yields the following expression for the gaussian time evolution:

$$e^{iH_st}|i(0)\rangle=\exp[i\alpha(t)(X-X_s(t))^2+iP_s(t)(X-X_s(t))+i\gamma(t)] \tag{5}$$

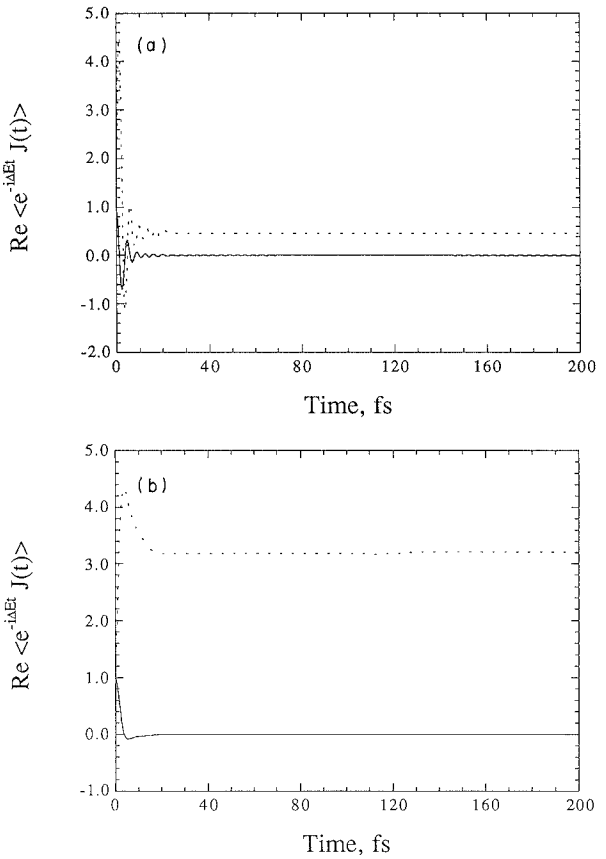

Fig. 5. $\langle \exp[-i\Delta E t]J(t)\rangle$ for (a) the HMB/TCNE and (b) the Ru/Fe charge transfer systems, with both 200 cm^{-1} inhomogeneous gap modulation and a 1 cm^{-1} solvent mode ($\lambda_{sol}=2300$ cm^{-1}) added (see text). Integrals are (a) 0.272 fs and (b) 4.46 fs. Trajectories are chosen at $T=0$ K. Solid lines represent the averaged integrand $\langle \exp[-i\Delta E t]J(t)\rangle$, while the broken line is a running sum of the integrand (as seen in ^{1}H NMR plots, for example). Note that the integral is unchanging after 50 fs in both cases; see Table 2 for integrated rates.

It is convenient to work in reduced coordinates defined (with $\hbar \equiv 1$) by

$$\hat{X} = Xm^{1/2} \tag{6a}$$

$$\hat{P} = Pm^{-1/2} \tag{6b}$$

and

$$\hat{\alpha} = \frac{\alpha}{m} \tag{6c}$$

Then,

$$e^{iH_s t}|i(0)\rangle = \exp[i\hat{\alpha}(t)(\hat{X}-\hat{X}_s(t))^2 + i\hat{P}_s(t)(\hat{X}-\hat{X}_s(t)) + i\gamma(t)] \tag{7}$$

The equations of motion for a harmonic surface, represented by normal modes {k}, are then [16]

$$\dot{\hat{X}}_k = \hat{P}_k \tag{8a}$$

$$\dot{\hat{P}}_k = -\omega_k^2 \hat{X}_k \tag{8b}$$

$$\dot{\hat{\alpha}}_k = -2\hat{\alpha}_k^2 - \tfrac{1}{2}\omega_k^2 \tag{8c}$$

$$\dot{\gamma}_k = \hat{P}_k^2 - E_k - \hat{\alpha}_k \tag{8d}$$

in which $\hat{X}_k$ is the deviation from the minimum in the kth direction and ω_k is the corresponding frequency. E_k is the energy in the mode k, so that the total energy E is given by

$$E = \sum_k E_k = \sum_k \tfrac{1}{2}[\omega_k^2 \hat{X}_k^2 + \hat{P}_k^2] \tag{9}$$

Analysis of resonance or near-resonance Raman spectra [13,14] provides unitless displacements D_k between the initial- and final-state surfaces, as well as frequencies ω_k. (Note that these values were obtained [13,14] assuming harmonic surfaces and no force-constant changes or mode mixing between ground and excited states, which is consistent with our model.) The contribution of mode k to the total reorganization energy λ (see Fig. 1) is $\lambda_k = 1/2\Delta_k^2\omega_k$, so that

$$\lambda = \frac{1}{2}\sum_k \Delta_k^2 \omega_k$$

This sum over k includes both inner shell and outer (solvent) modes. Initial conditions (for each coordinate k) are given by

$$\hat{\alpha}_k(0) = \frac{i}{2}\omega_k \tag{10a}$$

and

$$\gamma_k(0) = \frac{i}{4}\ln\left[\frac{\pi}{\omega_k}\right] \tag{10b}$$

The initial position and momentum are chosen randomly: for a given trajectory, a random number q in the range $0 \leqslant q \leqslant 2\pi$ is chosen, and $\hat{X}_k(0)$ and $\hat{P}_k(0)$ are assigned as follows:

$$\hat{X}_k(0) = \sqrt{2(n_k+\tfrac{1}{2})/\omega_k}\cos(q) \tag{11a}$$

and

$$\hat{P}_k(0) = -\sqrt{2\omega_k(n_k+\tfrac{1}{2})}\sin(q) \tag{11b}$$

This gives the proper total energy E for a given vibrational level $n=\{n_k\}$. Propagation of the wavepackets on the initial- and final-state surfaces is then straightforward, as is the evaluation of the rate. Except where indicated, we assume that initial- and final-state surfaces are described by the same characteristic frequencies, and we use the FGA of Heller [16b], in which the width term α is fixed in time ($\alpha(t)=i\omega/2$, the phase term γ is fixed as well). We relax these assumptions in Section 9 below.

4. Initial observations

The remainder of this text deals with the two-site, non-adiabatic ET model as applied to three systems. The first is a reduced-dimensionality model for the hexa-aquo-iron (2+/3+) self-exchange reaction, based on the analysis of Siders and Marcus [5], which describes the inner-shell (iron–oxygen stretch) motion as a single, averaged harmonic mode with $\hbar\omega_{in} = 431$ cm^{-1} (Table 1). We will address the additional solvent modes suggested by Siders and Marcus in Section 6 [5]. In Fig. 2, we show a plot of $e^{-i\Delta Et}J(t)$ at $T = 0$ K for this one-mode, two-site system (λ_i is the inner-shell reorganization energy). Since rate constants, like other linear transport coefficients, are clearly defined only when the system under study somehow incorporates dissipation, in the absence of external perturbations (*e.g.* dephasing, damping, gating, etc.), we observe recurrences, the integral in eqn. (4a) becomes divergent, and no rate can be defined [10,12]. This is, however, a model system, and real systems have many more active modes, which will act to remove recurrences on a reasonable time scale (*e.g.* 0.1–1 ps) via inner shell and solvent interactions. However, for all of our models, and indeed for any comparable models without dissipation, significant recurrences are still observed [16].

Markel *et al.* [13], and Barbara and co-workers [14] have each provided (via resonance and near-resonance Raman scattering measurements) a mode-by-mode analysis of the coupled vibrations in the ET reactions in the hexamethylbenzene/tetracyanoethylene charge transfer complex (HMB/TCNE) and the $(H_3N)_5$Ru-NC-Fe$(CN)_5^{1-}$ mixed-valence complex (Ru/Fe), respectively, including experimentally-derived equilibrium displacements and vibrational frequencies. These data permit the definition of a multimode harmonic double-minimum potential surface, incorporating the vibronic coupling (at the displaced oscillator level) to the many modes (11 and 8 for the HMB/TCNE and Ru/Fe systems, respectively). In Fig. 3, we plot $e^{-i\Delta Et}J(t)$ for these two systems. Again, these represent the systems as free molecules, with no solvent, and we again observe recurrences.

TABLE 1. Parameters for the Fe(2+/3+) charge-transfer system: frequencies, reorganization energies, and unitless equilibrium displacements for the one-mode or two-mode treatment (see text). $\Delta E = 0$

ω (cm^{-1})	λ (cm^{-1})	Δ
431	2969	3.68
389	1160	2.44
490	1840	2.74

For comparison, we note that in the molecular dynamics simulations of Maroncelli and co-workers [17] and Hynes *et al.* [18] on polar aprotic solvents such as acetonitrile, significant solvent reorganization occurs on a time scale of about 0.1 ps. We assume, therefore, that systems (such as those studied here) which exhibit recurrences of the time correlation function on time scales greater than 100 fs must be influenced by solvent motion. Even without this assumption, we must treat the solvent as a source of both (a) spectral line shifts and broadening, and (b) damping, brought about by the random interaction of the solvent with the solute. We shall first examine the spectral line broadening aspects of the solvent, and then combine this with the energy-accepting ability of the solvent.

5. Inhomogeneous spectral line broadening

The role of solvent damping and dephasing in producing spectral line broadening (both vibrational and electronic) in energy and proton transfer has been examined extensively [19,20]; such solvent effects are clearly crucial in any discussion of electron transfer [18,21].

Spectral line broadening can occur in a number of ways. The action of the solvent on a system affects the initial and final electronic state energies. This *gap modulation* is by far the most common form of broadening described in the current literature [21(b)], and we have chosen to focus on its role. Dephasing might also occur via random noise associated with the normal mode vibrational frequencies of the system, the equilibrium displacements of the electronic states, or the electronic matrix elements (breakdown of the Condon approximation).

Electronic gap modulation may have either inhomogeneous or homogeneous character [20,21(b),22], depending on the relative timescales of the experiment (in this case, ET) and the underlying gap fluctuations (*i.e.* fluctuations of the solvent matrix). In the limit of fluctuations that are much slower than the experiment, inhomogeneous broadening predominates, while homogeneous broadening predominates in the opposite limit. It is possible to distinguish experimentally between homogeneous and inhomogeneous broadening via optical-pulse and photon-echo techniques and non-linear experiments [20(b),21(b),23(b)].

In our model, inhomogeneous gap modulation is treated as follows. Inhomogeneous modulation is represented by an ensemble of trajectories, each with a distinct constant value of ΔE ($=\Delta E_{IF}$, the electronic energy gap), sampled from a Gaussian distribution characterized by

$$\langle \Delta E \rangle = \Delta E^* \tag{12}$$

and

$$\langle (\Delta E - \langle \Delta E \rangle)^2 \rangle = A^2 \tag{13}$$

Such a gaussian distribution is justified in the stochastic theory in the case of a large solute molecule or system surrounded by relatively small, closely packed solvent molecules; a lorentzian distribution applies in the opposite limit [20]. Homogeneous modulations are represented by a time-dependent stochastic energy gap for each trajectory.

We restrict our attention to (gaussian) inhomogeneous broadening, as though the ET systems were in frozen, glass-like matrices, for the sake of ease of calculation. The rate defined in eqn. (3), then, includes an average over ensemble, so that

$$\langle \Gamma_I \rangle = \left\langle \int dt e^{-i\Delta E t} C(t) \right\rangle \tag{14}$$

where we average over a gaussian distribution of ΔE. We also make the assumption that the experiment is complete on a finite timescale, and, using numerical integration techniques, the average of the integral is then equal to the integral of the average (of $e^{-i\Delta E t}C(t)$). We can then plot the average of $e^{-i\Delta E t}J(t)$ for systems with gap modulation (as in Figs. 4–6,8), and compare them to Fig. 3 (without gap modulation).

Figure 4 is a plot of $\langle e^{-i\Delta E t}J(t)\rangle$ for the HMB/TCNE and Ru/Fe systems ($T=0$ K), with inhomogeneous gap modulation added ($A=200$ cm^{-1}). The magnitude of the gap modulation here is arbitrary, but it is clear that such modulation affects the integrand of eqn. (3) dramatically: all recurrences beyond about 100 fs are effectively removed. The dependence of the averaged rate on A (for $A=100$–1000 cm^{-1}) for the Ru/Fe system ($T=0$ K) is given in Fig. 9; note that the rate decreases less than 10% over this range. (Suitable values for A for these, or similar, systems have not been reported.)

6. Treatment of solvent as additional modes

The solvent has an important role quite apart from being just a source of gap modulation. As shown above, it is far more common in the electron-transfer problem to treat the solvent as the source of polarization modes that couple with the system. This viewpoint was pioneered by Marcus [1]. A solvent must be treated both as a dynamic medium, characterized by random short-range motion (of solvent molecules) which leads to gap modulation but does not act to accept energy, and as an energy acceptor, adding significantly to the total reor-

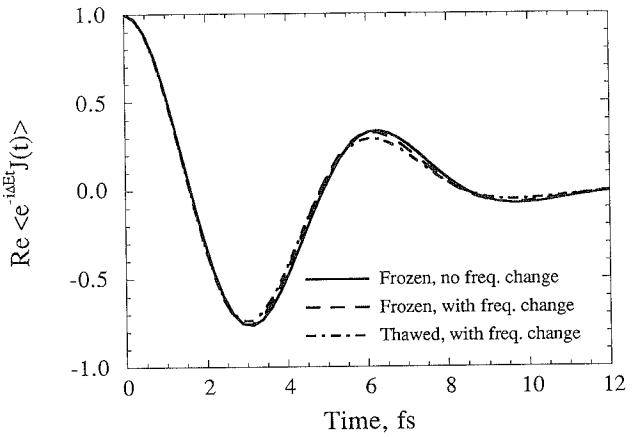

Fig. 6. Comparison of thawed *vs.* frozen wavepackets, and frequency-changing *vs.* non-frequency-changing surfaces, in the model hexa-aquo-iron self-exchange system. In all three cases, two solvent modes (1 and 170 cm^{-1}) are added (no recurrences were observed after 20 fs). Note that, for this symmetric system, all three treatments are basically identical, with similar integrals (differences are less than 10%). (See text and Fig. 7.)

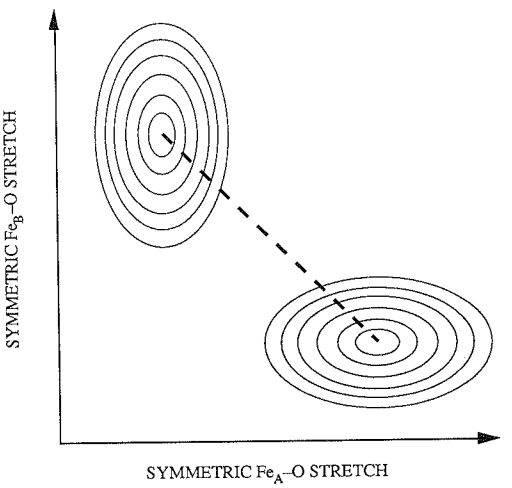

Fig. 7. Pictorial description of the hexa-aquo-iron (2+/3+) self-exchange reaction (characteristic frequencies: 389 and 490 cm^{-1}; see Table 1). When the electron is transferred, there are frequency changes corresponding to changes in oxidation states of the two iron centers. Siders and Marcus have approximated this two-mode system by a single energy-weighted average system of one mode (431 cm^{-1}). Then the reaction coordinate is given by the broken line (see text and Fig. 6). Here, the differences in frequency have been over-emphasized for clarity.

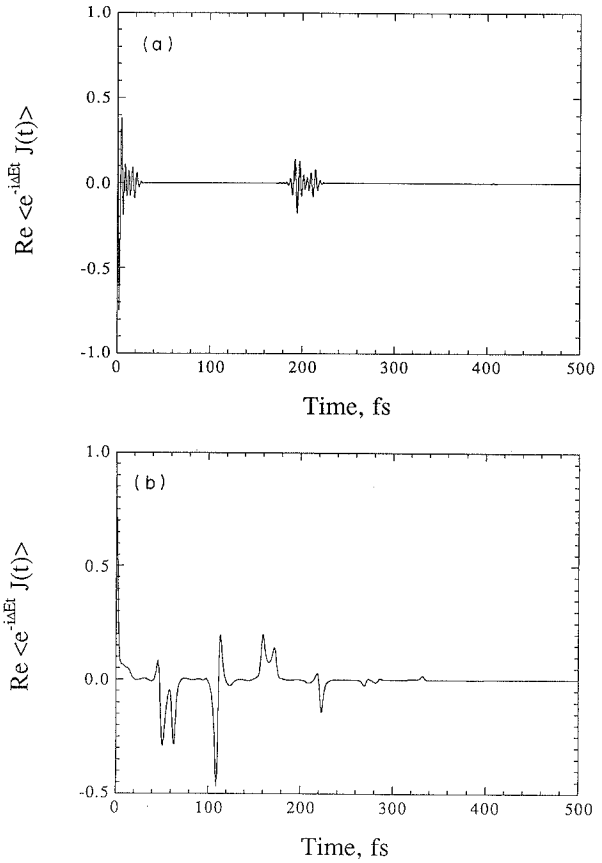

Fig. 8. Reduced-dimension treatment for the (a) HMB/TCNE and (b) Ru/Fe charge transfer systems. Here, the many-mode systems have been approximated by two modes, one high-frequency and one low-frequency, plus a single (frequency, 1 cm^{-1}; reorganization energy, 2300 cm^{-1}) solvent mode. Integrals are (a) 0.121 fs and (b) 5.89 fs. (See text and Fig. 5.)

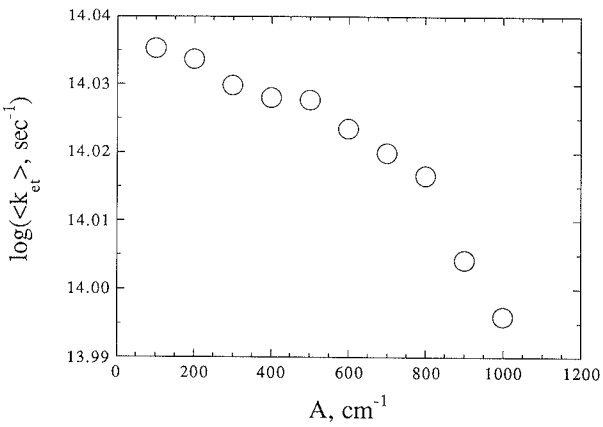

Fig. 9. Dependence of averaged rate ($T=0$ K) on gap modulation constant A (see text) for the Ru/Fe charge transfer system.

ganization energy of the electron-transfer process. Note that the treatment of the previous section fails to include the energy-accepting properties of the solvent, which can result in significant changes in rate calculations (see Table 2). (In the usual,

TABLE 2. Comparison of the present analysis with that of Fischer and van Duyne [8] including both the steepest-descents and numerical integration methods for rate determination, as well as experimental results. Rates are given in s^{-1}

	HMB/TCNE	Ru/Fe
Current work +200 cm^{-1} broadening	2.9×10^{11}	1.0×10^{14}
Current work +200 cm^{-1} broadening +1 cm^{-1} solvent mode	3.0×10^{12}	4.0 ± 10^{13}
Fischer/van Duyne steepest descents[a]	1.2×10^{13}	1.7 ± 10^{14}
Fischer/van Duyne numerical integration[b]	3.0×10^{12}	4.1 ± 10^{13}
Experiment[c]	$\sim10^{11}$	$\sim10^{13}$

[a]This includes a 1 cm^{-1} solvent mode and 200 cm^{-1} of inhomogeneous gap modulation (see text) [8].
[b]This includes a 1 cm^{-1} solvent mode and 200 cm^{-1} of inhomogeneous gap modulation. Numerical integration steps of about 0.04 fs (2 au) were sufficient for convergence [8].
[c]Refs. 14 and 25.

i.e. Marcus-type, picture, λ_0 or λ_{sol} enters *only* as an accepting mode.) A convenient way to represent the energy-accepting characteristics of the solvent is to include a finite series of harmonic oscillators with appropriate (solvent) frequencies and reorganization energies [21(b),23(a),23(b)], while the gap-modulation aspects are treated as in the previous section. Other groups have treated the solvent motion as a single, classical, overdamped oscillator [21(a)][†], but, in this treatment, we shall treat the solvent as an undamped oscillator.

In this simplest model treatment, we add a single-solvent mode with $\hbar\omega_{sol}=1$ cm^{-1} and $\lambda_{sol}=2300$ cm^{-1} [5,26]. This single-solvent mode is clearly a drastic misrepresentation and oversimplification, as evidenced by both simulations and neutron-scattering measurements on real liquids. We use it here as a zero-order model for largely historical reasons [5,26]; it represents the solvent as an energy acceptor, but fails to represent it in terms of proper electronic and nuclear motions[††]. In a more rigorous treatment, the 2300 cm^{-1} of reorganizational energy would be distributed among large, slow translational and ro-

[†]Lin and co-workers have, in an extensive and important series of papers, shown that the saddle-point method can be used in the context of a correlation-function approach to ET rates, to examine such effects as temperature dependence, anharmonicity, and frequency changes. See, for example, ref. 24.

[††]A more general and reasonable approximation for the single solvent mode frequency is provided by R.R. Dogonadze and Z. Urushadze [26(d)]. See also B.S. Brunschwig *et al.* [26(e)].

tational motions, faster librational and vibrational motions, and very fast electronic motions. Such a treatment (which would generally be based on the use of molecular dynamics simulations [23(c)] to obtain the appropriate spectral density [23(c),23(d)]) would also make unnecessary the use of inhomogeneous or homogeneous gap modulation, as it would be accounted for by a distribution of solvent configurations and motions. Representing the solvent by a single 1 cm^{-1} mode allows the (model) solvent to act only as a slow damping process, in addition to its energy-accepting ability. In spite of its obvious limitations, this solvent approximation serves to illustrate our method.

Addition of this single low-frequency mode to the HMB/TCNE and Ru/Fe systems gives results shown in Fig. 5, with gap modulation ($A = 200$ cm^{-1}) added. Qualitatively, the additional solvent mode acts to damp out recurrences in a manner similar to that of the gap modulation alone (Fig. 4); however, the integrated rates differ between the two methods (see Table 2). In the case of the HMB/TCNE ET system, the rate is increased about tenfold, as the additional solvent reorganization energy makes the system less inverted (ΔE is closer to λ_{tot}), while in the Ru/Fe system (which lies in the normal regime), the rate decreases by about five times (see Section 7 and Table 2 below). This is as expected from the Marcus-like factor $\exp[-(\Delta+\lambda)^2/(4\lambda kT)]$.

It should be noted here that our treatment of the solvent in terms of two distinct mechanisms, as a source of random modulations of ΔE and as a significant contribution to λ_{tot} (and therefore as an energy acceptor), can be understood in terms of the proton-transfer work of Hynes and coworkers [10]. They employed a cumulant expansion of a time-dependent flux correlation function, and found that the solvent influence on the proton transfer rate can be decomposed into two distinct mechanisms: a direct mechanism which concerns the interaction of the solvent with the proton charge (as well as the charges of the solute molecule) and appears in the modulation of ΔE (thus, a source of gap modulation), and an indirect one which enters via a damping, energy-accepting mechanism [10].

7. Electronic coupling matrix element and calculation of rates

Experimental methods for an estimation of V_{IF} include the Hush–Mulliken analysis [27], which makes use of the oscillator strength for the inter-valence optical transition, and the electrochemical method developed by Curtis *et al.* [28]. The Hush–Mulliken analysis [27] relies on knowledge of the ET distance for the optical ET transition, and (typically) the metal-to-metal atomic distance (in the case of a bimetallic inter-valence ET system) is used:

$$|V_{IF}| = 2.06\times10^{-2}\,\frac{(\epsilon_{max}\Delta\bar{\nu}_{1/2}E_{op})^{1/2}}{eR} \qquad (15)$$

in which ϵ_{max} (M^{-1} cm^{-1}) is the extinction coefficient of the inter-valence absorption, $\Delta\nu_{1/2}$ (cm^{-1}) is the full width at half maximum, E_{op} (cm^{-1}) is the optical energy of the ET transition, e (unitless) is the amount of charge transferred, and R (Å) is the charge-transfer distance. This can result in an underestimation of V_{IF} due to an overestimation of R (or, alternately, an overestimation of e) [28(b)]; for example, the recent work of Oh and Boxer [29] indicates that the actual distance for inter-valence transfer in the $(H_3N)_5$Ru-4,4′-bipyridine-Ru$(NH_3)_5^{5+}$ mixed-valence complex is only about 45% of the geometric distance between the metal centers.

Understanding the limitations of the Hush–Mulliken analysis, we have calculated the electronic coupling element in the HMB/TCNE system to be 3500 cm^{-1} (with the implication that this is a lower limit; parameters for eqn. (15) were estimated from the optical absorbance spectrum reported by Markel *et al.* [13], and a charge transfer distance of 4 Å was used as a high limit[†,††]). We

[†]It is interesting to note that the outer-shell reorganization energy used here, 3900 cm^{-1}, is nearly twice that suggested by Marcus, and that if we use 2300 cm^{-1} as the (outer-shell) reorganization energy, we get a rate of about 10^{12} s^{-1} (10^{13} for the Fischer–van Duyne steepest-descents analysis). It should be noted that the fluorescence decay measurements may give rates which are far from those of thermal systems, as the thermal transfer occurs from an initial state which is at thermal equilibrium, whereas that in the fluorescence experiment is most likely far from such an equilibrium. It is also very important to note that, in the HMB/TCNE system, the broad absorbance band most likely consists of (at least) two closely spaced transitions, and that therefore the outer-shell reorganization energy given by Myers is probably an overestimation. Again, this is an extremely inverted reaction ($\Delta E_{experimental} = 11\ 600$ cm^{-1}).

[††]A geometry minimization on Gaussian-92 was performed on the HMB/TCNE system, using an STO-3G basis set, and the following constraints: the HMB and TCNE fragments were coplanar; the non-protonated core of the HMB had D_{6h} symmetry; the TCNE had D_{2h} symmetry; each CH_3 fragment had C_{3v} symmetry. The intermolecular distance was then calculated to be 3.89 Å: thus, our upper limit of 4 Å is not unreasonable. According to crystal structures, the intermolecular distance (in the crystal, subject to packing forces) is 3.35 Å [30], and is most likely a lower limit of the intermolecular distance. However, the distance noted in eqn. (15) is the distance over which the effective charge is transferred; if we take this to be one electron, then (as noted) the distance may be much shorter than even the crystal structure predicts.

use the experimentally obtained V_{IF} of Dong and Hupp [28(b)] (3200 cm^{-1}) for the Ru/Fe ET system. It should be noted that these couplings obviously correspond to adiabatic systems, while our model is based on *non*-adiabatic ET. Clearly, this is inconsistent; however, we make use of these systems and these data simply to illustrate the treatment.

Results of rate calculations at $T=0$ K for the HMB/TCNE and Ru/Fe ET systems, both with the gap-modulation treatment of Section 5 and the additional 1 cm^{-1} solvent mode of Section 6, are indicated in Table 2. For comparison, rates calculated using the steepest-descents method of Fischer and van Duyne [8] (also at $T=0$ K) are included. Also, Fig. 10 gives a comparison of this simplest model (gap modulation ($A=200$ cm^{-1}) and solvent mode ($\hbar\omega_{sol}=1$ cm^{-1} and $\lambda_{sol}=2300$ cm^{-1}) added) with the method of Fischer and van Duyne for a range of electronic separation of initial and final states (ΔE) in the HMB/TCNE system (experimentally obtained ΔE is indicated in the figure by a vertical line [13]). Note that both methods give the expected inverted region effects on rates [31], including the expected non-quadratic behavior for a multi-mode energy gap [32,33].

Note, too, that the inner and outer shell reorganization energies are properly included ($\lambda_i=3515$ cm^{-1}, $\lambda_{sol}=2300$ cm^{-1}; again, this outer shell (solvent) reorganization energy is from the single-mode solvent approximation used in Section 6)†. Both in Table 2 and Fig. 10, we observe that the steepest-descents method gives rates which are about ten times larger than those of our model. The steepest-descents method uses a stationary phase approximation to calculate the rate integral, and, in so doing, yields larger rates than those calculated with our analysis. To evaluate an exponential function by steepest descents, one approximates as [8,24]

$$\int_{-\infty}^{\infty} dt\ e^{f(t)} \cong \int_{-\infty}^{\infty} dt\ \exp\left[f(t)|_{t_s} + \left.\frac{\partial f(t)}{\partial t}\right|_{t_s} (t-t_s) + \frac{1}{2}\left.\frac{\partial^2 f(t)}{\partial t^2}\right|_{t_s} (t-t_s)^2 \right] \tag{16}$$

dropping terms higher than second derivative, which yields an easily integrated gaussian function. Choosing the saddle point t_s such that

$$\left.\frac{\partial f(t)}{\partial t}\right|_{t_s} = 0 \tag{17}$$

and then

$$Re \int_{-\infty}^{\infty} dt\ e^{f(t)} \cong e^{f(t_s)} \left(\frac{2\pi}{|\partial^2 f/\partial t^2|_{t_s}} \right)^{1/2} \tag{18}$$

the rate is then given by

$$k_{et} = V_{IF}^2\ e^{f(t_s)} \left(\frac{2\pi}{|\partial^2 f/\partial t^2|_{t_s}} \right)^{1/2} \tag{19}$$

in which (at $T=0$ K)

$$f(t_s) = i\Delta E_{IF} t_s - \sum_j \frac{\lambda_j}{\omega_j} [1 - e^{-i\omega_j t_s}] \tag{20}$$

where ω_j and λ_j refer to the frequency and reorganization energy corresponding to mode j, and (again) we use $\hbar=1$ [24]. Note that the steepest-descents method fails at $\Delta E \approx 0$ (if $T=0$ K).

As an alternative to making the steepest-descents approximation of eqn. (16), we have explicitly evaluated the left-hand side of eqn. (16) using numerical integration [34] and appropriately small time steps (2 au). Here, $f(t)$ is given by eqn. (20), in which t_s is replaced by t; inhomogeneous broadening (in the same manner as described in Section 5) and a single solvent mode (as described in Section 6) are included, and this treatment is

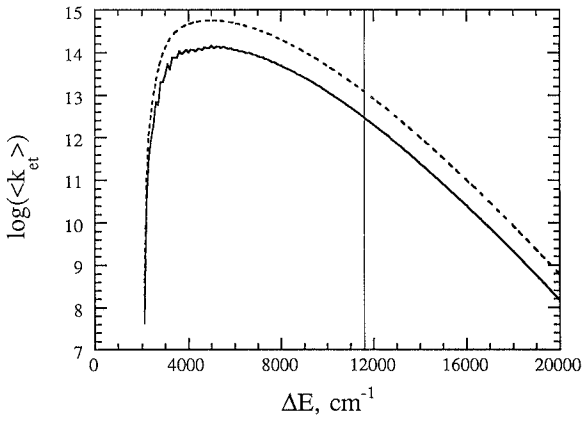

Fig. 10. $\log\langle k_{et}\rangle$ (s^{-1}) *vs.* ΔE for the HMB/TCNE charge transfer system, with an additional 1 cm^{-1} (solvent) mode with $\lambda_{sol}=3900$ cm^{-1} (from Markel *et al.* [13]) and 200 cm^{-1} inhomogeneous gap modulation. Solid line represents the time-dependent golden-rule (TDGR) formulation, while the broken line represents the steepest-descents (SD) method of Fischer and van Duyne (see text and ref. 8). The vertical line represents the experimentally measured ΔE for this system. (The noise associated with the TDGR treatment is the result of numerical integration error.)

†Note that the treatment of Bosma *et al.* includes gap modulation along with the overdamped oscillator. We can do this in our model as well, although the treatment of the solvent as an overdamped oscillator may be inappropriate.

compared with both the steepest-descents approximation (also with broadening and solvent mode added to the expression for $f(t_s)$ in eqn. (20), and also evaluated using numerical integration [34]) and our model.

The steepest-descents approximation for the HMB/TCNE plus single-solvent mode and 200 cm^{-1} broadening (as indicated in Table 2) gives a rate of 1.20×10^{13} s^{-1}, while an explicit treatment of the same expression (no steepest-descents approximation) gives an integrated rate of 3.0×10^{12} s^{-1}, in agreement with our time-dependent formulation. (For this simplest case of displaced harmonic oscillators, our time-dependent wavepacket treatment should be exact, and must agree with the polaron theory result.) Thus, it seems the steepest-descents approximation overestimates the rate by about five times for this particular system. (Similar results are observed for the Ru/Fe system; see Table 2.) Variation by less than a factor of ten, over a force constant range of more than seven orders of magnitude, demonstrates that the steepest-descents approximation scheme works quite well for this situation of multiple modes and a substantial energy gap.

8. Temperature effects

Figure 11 indicates the effects of temperature on the single-mode model Fe (2+/3+) self-exchange system, indicating $\langle e^{-i\Delta E t}J(t)\rangle_T$ (average over a Boltzmann distribution) for $T=0$, 100 and 1000 K. Here, trajectories were defined according to eqn. (11), in which n was chosen randomly for each trajectory based on probabilities according to a Boltzmann distribution. Note that, in the case of a purely harmonic system, recurrences are still observed; however, raising the temperature narrows the recurrences. The effects of temperature on rate can best be described by Figs. 12 and 13. In Fig. 12(a), at the $T=0$ K limit, only the ground-state vibrational level on surface I is populated. As the temperature is raised, the rate increases as the vibrational levels closer to the crossing point ($E_n \approx \lambda_{tot}$) between the electronic surfaces (which have small Franck–Condon barriers) become populated. Then, as even higher levels become populated (Fig. 12(c)), the rate tends to drop again, as levels which are much higher than the crossing point ($E_n \gg \lambda_{tot}$) have larger Franck–Condon barriers. If the system is in the normal (non-inverted) region, we see that the rate increases with temperature as shown in Fig. 13(a) for the Fe (2+/3+) system ($\Delta E=0$; two solvent modes of 1 and

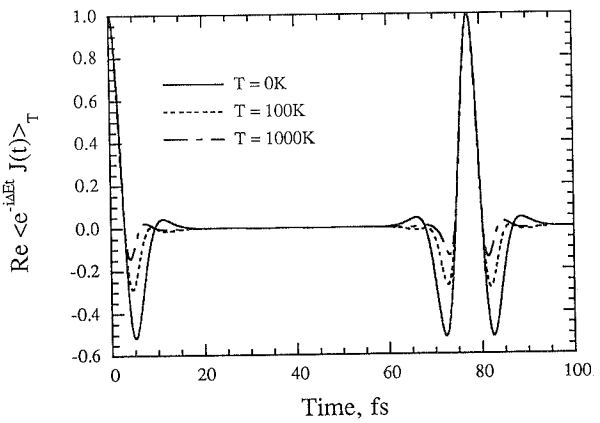

Fig. 11. Comparison of integrands of the one-mode (431 cm^{-1}) system of Fig. 2 at 0, 100, and 1000 K (see text) (200 trajectories). Note that the width and amplitude of the recurrences are narrowed at higher temperatures.

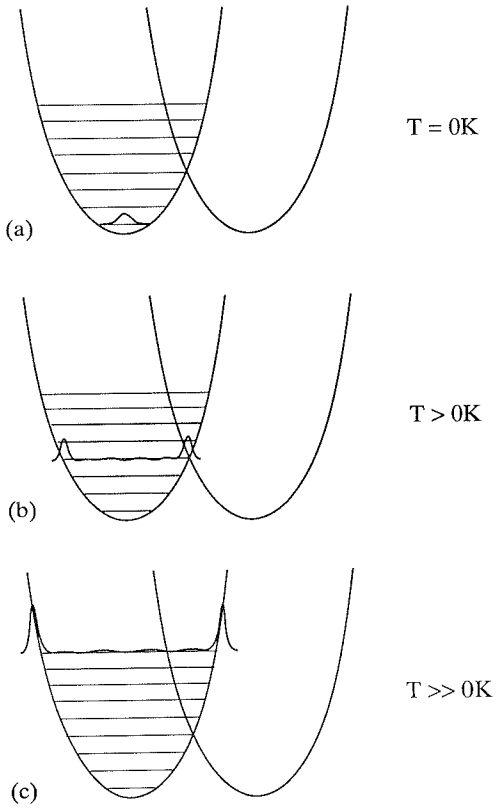

Fig. 12. Pictorial description of temperature effects on rate for a degenerate system. At $T=0$ K (a), only the $n=0$ vibrational level is populated, and Franck–Condon overlaps are small. At $T>0$ (b), levels closer to the crossing point become populated, and the average rate increases. As higher levels become populated ($T\gg0$) (c), the rate drops again, as higher vibrational states again have smaller Franck–Condon overlaps with the final-state surface. The curves depicted are sketches of (Y^2).

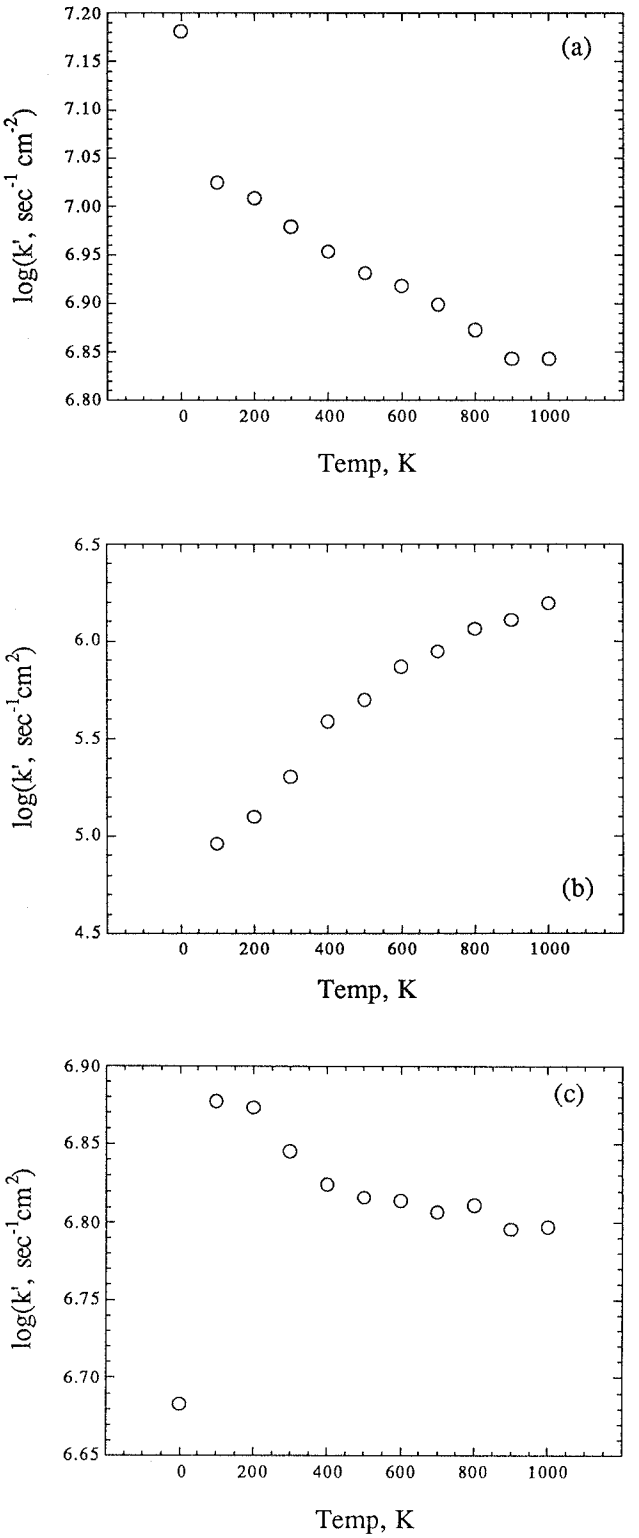

Fig. 13. log(averaged rate) *vs.* temperature for the three-mode model system (frequencies are 1, 170 and 431 cm^{-1}; corresponding reorganization energies are 770, 1487 and 2926 cm^{-1}); includes 200 cm^{-1} inhomogeneous gap modulation. (a) Degenerate system. (b) Crossing point ($\Delta E = \lambda_{tot}$). (c) Inverted by 1800 cm^{-1}. The initial jump comes from population of many levels of the 1 cm^{-1} mode with $T = 100$ K, as opposed to the relatively restricted motion of the initial-state wavepacket at $T = 0$ K.

170 cm^{-1} added [5]). If the system is at the crossing point ($\Delta E = \lambda_{tot}$), raising the temperature causes the rate to drop as the ground vibrational state becomes depopulated, as seen in Fig. 13(b). If the system is not far from the crossing point, raising the temperature (as described above) first increases the rate, then decreases it, as shown in Fig. 13(c) (1800 cm^{-1} in the inverted region).

Temperature effects are not very large, however: note that, over the range 0–1000 K, the rates change, for this particular system, less than an order of magnitude. (For comparison, the Ru/Fe system is in the normal (non-inverted) regime, close to the crossing point, while the HMB/TCNE system is well into the inverted region. The Fe (2+/3+) self-exchange system is degenerate, except where artificially modified, as above.) The widths of the wavepackets are temperature-dependent [15], which may slightly affect the rate, but we have not examined such dependence here.

9. Frequency changes

If we project a wavepacket defined by one surface (say, the initial-state surface) onto another surface (say, the final-state surface) defined by different frequencies, several changes are expected. Because the potential surface slopes change, the rate of translation of the product wavepacket will change. Also, $\alpha(t)$ is no longer necessarily equal to $\alpha(0)$ (see eqn. (5)), and the width of the wavepacket becomes time-dependent ("thawed"). In addition, if the surface is not harmonic (*e.g.* Morse), α will, in general, be time-dependent, and the gaussian will "fracture" near the inner turning point. We address the possibility of frequency changes here, which typically occur in any non-symmetric system, and leave anharmonicities for a later paper.

We compare here the frozen wavepacket approximation, with and without frequency changes, with propagation of thawed wavepackets (see Section 3 for a definition of frozen and thawed gaussian wavepackets). A simple example is the model of Siders and Marcus for the Fe (2+/3+) self-exchange [5], in which, rather than approximate the two frequencies corresponding to Fe(2+)–oxygen and Fe(3+)–oxygen stretching modes by an average 431 cm^{-1} mode, we use the two frequencies of 389 and 490 cm^{-1} for Fe(2+) and Fe(3+), respectively [5]. It should be clear that there is a frequency change involved when going from the initial-state surface to the final-state surface: when the electron is transferred, the characteristic frequency of the donor iron becomes

that of the acceptor, and *vice versa*. We have surfaces which can be represented by the two (exaggerated) ellipsoids of Fig. 7 — the initial-state surface and the final-state surface are displaced in both coordinates, and are rotated 90° relative to each other. The broken line represents the (averaged) 431 cm^{-1} approximation.

For comparison of rates, we have added two additional (solvent) modes, described by Siders and Marcus [5], with characteristic frequencies of 1 and 170 cm^{-1} (corresponding reorganization energies are 770 and 1487 cm^{-1}; we assume that these frequencies and reorganization energies do not change upon transfer). Figure 6 gives a comparison of the frozen, four-mode (two internal and two solvent) system with the thawed (see Section 4.4) version of the same system, as well as the (frozen) four-mode (two 431 cm^{-1} modes and two solvent modes) system. Note that no *significant* differences are apparent, and that the integrals are basically identical (less than 10% difference).

The reason for the very small effect of frequency changes here is simply the choice of physical system: the symmetric $Fe^{2+}/Fe^{3+} \rightarrow Fe^{3+}/Fe^{2+}$ ET reaction has one frequency increasing at the same time that the other decreases the same amount, so that the net effect is very small. Figure 6 shows that the correlation functions at short time do differ, but only very slightly. (The correlation function at $t > 20$ fs has decayed to the point where it does not significantly contribute to the overall rate, in all three cases of Fig. 6.) Major differences will occur for ET reactions in which such compensating frequency changes do not occur, such as between a metal complex and an organic. Calculations on such systems are in progress[†].

10. Approximate vibrational representations

In the studies of betaine-30 by Walker *et al.* [37], they combine the models of Sumi and Marcus [38] and Jortner and Bixon [39] to yield a model for the calculation of ET rates in solution which breaks the reorganization energy into three parts: λ_{qm}, $\lambda_{cl,vib}$, and λ_{sol}, for a high-frequency, quantal-vibrational (internal) mode, a low-frequency, classical vibrational (internal) mode, and a classical solvent mode. In the HMB/TCNE ET system, Markel *et al.* [13] found that two modes, a low-frequency D–A stretch at 165 cm^{-1} and a high-frequency TCNE mode at 1551 cm^{-1}, make up about 60% of the total (internal) reorganization energy for the ET event (out of 11 internal modes), lending some credence to the two-internal-mode approximation of Walker *et al.* However, in studies of photoinduced ET in the Ru/Fe mixed-valence complex, Barbara and co-workers [14] found eight active modes, with three predominating (at 2104 cm^{-1}, 603 cm^{-1}, and 270 cm^{-1}, making up 75% of the total internal reorganization energy), suggesting that including the internal modes as only one fast and one slow mode may be an oversimplification. On the other hand, rate measurements of the ET reaction give an estimate [14] of τ_{et} (the half-life of the electron-transfer reaction) about 50 fs, suggesting that modes of less than 500 cm^{-1} may not be active in this transition, and thus two modes might adequately describe the ET.

To compare with the two-(internal)-mode analysis of Walker *et al.* [37], we have approximated the HMB/TCNE and Ru/Fe systems by two modes each (plus a single solvent mode), and we show $e^{-i\Delta Et}J(t)$ for each system in Fig. 8. We distribute the total internal reorganization energy λ_i between the two modes with the highest contributions to λ_i, according to their relative contributions. Thus, in the case of the HMB/TCNE charge-transfer complex, we have approximated 11 modes with $\lambda_i = 3515$ cm^{-1} by two modes, $\hbar\omega_1 = 165$ cm^{-1} and $\hbar\omega_2 = 1551$ cm^{-1}, with $\lambda_1 = 2097$ cm^{-1} and $\lambda_2 = 1418$ cm^{-1}; $\Delta E_{IF} = 11\,600$ cm^{-1}. In the case of the Ru/Fe mixed valence complex, $\lambda_i = 3220$ cm^{-1}; however, *three* modes contribute almost equally to 75% of λ_i. With the understanding that t_{et} is on the order of 50 fs, we approximated the eight modes of this system by the two modes with the largest contributions to λ_i which are greater than 500 cm^{-1}: $\hbar\omega_1 = 603$ cm^{-1} and $\hbar\omega_2 = 2104$ cm^{-1}, with $\lambda_1 = 1640$ cm^{-1} and $\lambda_2 = 1580$ cm^{-1}; $\Delta E_{IF} = 3000$ cm^{-1}. In addition, we have added a single solvent mode with $\hbar\omega_1 = 1$ cm^{-1} and $\lambda_{sol} = 2300$ cm^{-1}.

Comparing Figs. 5 and 8, we observe similar but distinct behavior. In the case of the HMB/TCNE system, recurrences are seen in both the 11-mode (Fig. 5(a)) and two-mode (Fig. 8(a)) cases at similar times, characterized by the slower, 165 cm^{-1} mode. Similarly, regular recurrences are seen in the Hupp and Barbara system, but the eight-mode case (Fig. 5(b)) is dominated by the 270 cm^{-1} mode, while the two-mode case (Fig. 8(b)) is dominated by the 603 cm^{-1} mode, which results in recurrences of much higher amplitude at much shorter times. In both cases, we see that the additional modes in Fig. 5 reduce the amplitudes

[†]The possible importance of frequency changes on ET rates has been stressed by Kakitani and Kakitani [35(a)] and by Ulstrup and Jortner [35(b)]. Effects of frequency changes have been calculated by Lin [36(a)], by Lagos and Friesner [36(b)], and by Chan and Page [36(c)].

of the recurrences seen in Fig. 8. In addition, integrals (over the ranges shown in the figures) are as follows: Fig. 5(a) *vs.* Fig. 8(a), 0.272 *vs.* 0.121 fs, and Fig. 5(b) *vs.* Fig. 8(b), 4.46 *vs.* 5.89 fs. The two-(inner-shell)-mode approximation is clearly inadequate where several modes define the recurrences (compare Figs. 5(b) and 8(b)); the other modes (with smaller contributions to the total reorganization energy) serve to make slight changes in the amplitude of the recurrences (compare Figs. 5(a) and 8(a)). Note that small contributions to the total reorganization energy equate with small normal-mode equilibrium displacements ($\Delta_k = (2\lambda_k/\omega_k)^{1/2}$), and the smaller the Δ_k, the less the overlap of the wavepackets is influenced by motion in coordinate k in time (as displacements along coordinate k are small).

Reduced pictures, involving one classical and one or two quantum degrees of freedom, are attractive both because they lead to semianalytic forms for the rate constant [26(b)], and because they are more easily interpreted than the full multi-mode quantum treatment. As we have demonstrated here, however, such reduced treatments can often lead to errors due to oversimplification of the true energy-flow dynamics.

11. Comments

We have demonstrated a new dynamical analysis of a slightly generalized non-adiabatic electron transfer (polaron) model which connects directly to experiment via resonance Raman studies, or to theoretical normal-mode analyses. It is related to, but distinct from, the correlation-function analysis of Fischer and van Duyne [3–8,11,26]: it views the electron transfer process from a purely dynamical point of view and allows for mode-by-mode analysis, but in a different manner, allowing for easy inclusion of effects such as solvent damping or frequency changes. It is substantially different from the Marcus–Hush transition-state theory [1,2], in that nuclear tunneling is included. We have examined the effects of solvent, temperature, and frequency changes on the model, as well as a two-mode approximation method for the vibronic coupling (in Section 10).

In general, in the absence of damping or dephasing processes, we observe recurrences (Figs. 2 and 3) whose amplitudes and periods are defined by the modes with the largest unitless equilibrium displacements (Δ_k). Inclusion of gap modulation or solvent modes removes these recurrences and allows the calculation of rates (Figs. 4,5,9 and 10 and Table 2); the addition of solvent modes with large reorganizational energies properly includes the energy-sink effects of the solvent. An examination of rate *vs.* ΔE_{if} gives the expected (according to Marcus–Hush [1,2]) inverted-region effects (Fig. 10). Temperature and frequency change effects are demonstrated in Figs. 13 and 6 respectively, and are found to be respectively small (but non-monotonic and not activated) and minimal. The observed temperature dependence is similar to that observed in a small-polaron model [4–8] (weak, monotonic and non-activated), and is substantially different from the temperature dependence predicted by transition-state theories [1,2] (activated), owing to the inclusion of nuclear tunneling (in the present model). The approximation of the many-mode systems described by two (one high-, one low-frequency) modes is found, in general, to be inadequate to describe rates, based on a comparison with the many-mode systems.

The model hamiltonian involves linear coupling between the vibrational coordinates and the electronic occupations [3–8,26]. This treats the inner-sphere reorganization effects exactly, within a harmonic approximation. The outer-sphere reorganization energy, and, more generally, the effects of the solvent, have been treated using several crude models. These models include

a. a simple dephasing picture, in which solvent fluctuations randomly modulate the exoergicity;
b. one-mode or two-mode harmonic approximations to the solvent coupling [5];
c. assuming that the solvent merely provides a thermostat, establishing a temperature in the inner-sphere modes.

More explicit modeling [10,17,18] of the solvent behavior can be added to our dynamical picture for the inner-sphere behavior; for example, we can couple to a molecular dynamics solvent description [15].

We used our models to calculate rates for the Hupp and Barbara Ru/Fe charge transfer system [14] and the Gould and Myers HMB/TCNE system [13] (indicated in Table 2). Estimations from experimental results are on the order of 10^{13} and 10^{11} s^{-1} [14,25], respectively. Thus, we are very close to the measured rate for the Ru/Fe ET system, while we overestimate the rate for the HMB/TCNE system by about ten times. It should be noted that the rate given for the HMB/TCNE system is from a fluorescence decay measurement, and is therefore not a "true" thermal rate [25].

It has been suggested that high-frequency modes (about 3500 cm^{-1}) with relatively small equilibrium displacements (Δ) may not be apparent in the

resonance Raman spectra but may significantly affect the rate. As a test of this hypothesis, a 3500 cm^{-1} mode was added to the HMB/TCNE + single (1 cm^{-1}) solvent mode system (see Table 2). With $\Delta = 0.05$ ($\lambda = 4.4$ cm^{-1}), the measured rate was 3.0×10^{12} s^{-1}, basically identical to the measured rate of the HMB/TCNE + 1 system without the high-frequency mode. With $\Delta = 0.5$ ($\lambda = 440$ cm^{-1}) (well within the realm of the resonance Raman experiment, as many of the 11 modes measured had Δ values in the range 0.5–0.6), the measured rate was 8.5×10^{12} s^{-1} — a fairly minor change in the rate, given the size of Δ. Our conclusion, therefore, is that high-frequency modes which are not observed in the resonance Raman spectrum (*e.g.* C–H stretches) do not significantly affect the rate.

This analysis of the simple non-adiabatic polaron model for ET has proven to be extremely versatile. Future steps include calculation of rates of optically induced charge transfer, in which the initial state is prepared by an optical excitation, addition of vibrational levels on the bridge state in the superexchange (three-site) model, anharmonic surfaces (*e.g.* Morse potentials), and calculation of absorption spectra.

Acknowledgments

MDT gratefully acknowledges a pre-doctoral fellowship from the National Science Foundation, and post-doctoral fellowships from the SNF (Denmark) and the American Scandinavian Foundation (USA). MAR and JTH are grateful to the Office of Naval Research and the Basic Energy Sciences Office of the US Department of Energy (Grant No. DE-FG02-87ER13808), respectively, for partial support of this research. AN thanks the Israel Academy of Science for partial support of this work. Thanks also go to G. Schatz and K. Mikkelsen for helpful discussions.

References

1 (a) R.A. Marcus, *J. Chem. Phys., 24* 966, 979 (1956); (b) R.A. Marcus, *J. Chem. Phys., 43* (1965) 679; (c) R.A. Marcus, *Rev. Mod. Phys., 65* (1993) 599.
2 (a) N.S. Hush, *Trans. Faraday Soc., 57* (1961) 557; (b) N.S. Hush, *Electrochim. Acta, 13* (1968) 1005.
3 J. Ulstrup and J. Jortner, *J. Chem. Phys., 63* (1975) 4358.
4 J. Jortner, *J. Chem. Phys., 64* (1976) 4860.
5 P. Siders and R.A. Marcus, *J. Am. Chem. Soc., 103* (1981) 741.
6 (a) S. Rackovsky and H. Scher, *J. Chem. Phys., 89* (1988) 7242; (b) H. Scher and T. Holstein, *Phil. Mag. B, 44* (1981) 343.
7 (a) N.S. Hush, *J. Phys. Chem., 90* (1986) 3657–3862; (b) K.V. Mikkelsen and M.A. Ratner, *Chem. Rev., 87* (1987) 113; (c) K.V. Mikkelsen and M.A. Ratner, *J. Phys. Chem., 93* (1989) 1759; (d) K.V. Mikkelsen and M.A. Ratner, *J. Chem. Phys., 90* (1989) 4237; (e) R. Kosloff and M.A. Ratner, *Israel J. Chem., 30* (1990) 45; (f) M.D. Newton, *Chem. Rev., 91* (1991) 767; (g) S.S. Isied, M.Y. Ogawa and J.F. Wishart, *Chem. Rev., 92* (1992) 381; (h) K.D. Jordan and M.N. Paddon-Row, *Chem. Rev., 92* (1992) 395.
8 (a) R.P. van Duyne and S.F. Fischer, *Chem. Phys., 5* (1974) 183; (b) S.F. Fischer and R.P. van Duyne, *Chem. Phys., 26* (1977) 9; (c) W. Knapp and S.F. Fischer, *J. Chem. Phys., 89* (1988) 3394.
9 T. Yamamoto, *J. Chem. Phys. 33* (1960) 281; D. Chandler, *J. Chem. Phys., 68* (1978) 2959; G.A. Voth, D. Chandler and W.H. Miller, *J. Phys. Chem., 93* (1989) 7009; X. Song and A.A. Stuchebrukhov, *J. Chem. Phys., 99* (1993) 969; D. Borgis and J.T. Hynes, *J. Chim. Phys. (Paris), 97* (1990) 819.
10 (a) D. Borgis and J.T. Hynes, *J. Chem. Phys., 94* (1991) 3619; (b) S.J. Klippenstein and J.T. Hynes, *J. Phys. Chem., 95* (1991) 4651.
11 G.C. Schatz and M.A. Ratner, *Quantum Mechanics in Chemistry*, Prentice-Hall, Englewood Cliffs, NJ, 1993, Chaps. 9 and 10.
12 M.D. Todd, A. Nitzan and M.A. Ratner, *J. Phys. Chem., 97* (1993) 29.
13 F. Markel, N.S. Ferris, I.R. Gould and A.B. Myers, *J. Am. Chem. Soc., 114* (1992) 6208.
14 (a) G.C. Walker, P.F. Barbara, S.K. Doorn, Y. Dong and J.T. Hupp, *J. Phys. Chem., 95* (1991) 5712; (b) K. Tominaga, D.A.V. Kliner, A.E. Johnson, N.E. Levinger and P.F. Barbara, *J. Chem. Phys., 98* (1993) 1228; (c) D.A.V. Kliner, K. Tominaga, G.C. Walker and P.F. Barbara, *J. Am. Chem. Soc., 114* (1992) 8323.
15 (a) E. Neria, A. Nitzan, R.N. Barnett and U. Landman, *Phys. Rev. Lett., 67* (1991) 1011; (b) E. Neria and A. Nitzan, *J. Chem. Phys., 96* (1992) 5433.
16 (a) E.J. Heller, *J. Chem. Phys., 62* (1975) 1544; (b) E.J. Heller, *J. Chem. Phys., 75* (1981) 2923; (c) E. Neria and A. Nitzan, *J. Chem. Phys., 99* (1993) 110.
17 (a) M. Maroncelli, *J. Chem. Phys., 94* (1991) 2084; (b) M. Maroncelli and G.R. Fleming, *J. Chem. Phys., 89* (1988) 5044; (c) E.W. Castner, G.R. Fleming, B. Bagchi and M. Maroncelli, *J. Chem. Phys., 89* (1988) 3519; (d) M. Maroncelli, J. MacInnis and G.R. Fleming, *Science, 243* (1989) 1674.
18 (a) D. Zichi, G. Ciccotti, J.T. Hynes and M. Ferrario, *J. Phys. Chem., 93* (1989) 6261; (b) R.A. Kuharski, J.S. Bader, D. Chandler, M. Sprik and M.L. Klein, *J. Chem. Phys., 89* (1988) 4248; (c) J.W. Halley and J. Hautman, *Phys. Rev. B, 38* (1988) 11704; (d) J.K. Hwang and A. Warshel, *J. Am. Chem. Soc., 109* (1987) 715; (e) P.F. Barbara, T.J. Kang, W. Jarzeba and T. Fonseca, *Jerusalem Symp. Quantum Chem. Biochem., 22 (Perspect. Photosynth.)* (1990) 273.
19 (a) M. Tuckerman and B.J. Berne, *J. Chem. Phys., 98* (1993) 7301; (b) P.F. Barbara, G.C. Walker and T.P. Smith, *Science, 256* (1992) 975; (c) G.C. Walker, E. Aakesson, A.E. Johnson, N.E. Levinger and P.F. Barbara, *J. Phys. Chem., 96* (1992) 3728; (d) E. Åkesson, G.C. Walker and P.F. Barbara, *J. Chem. Phys., 95* (1991) 4188; (e) U. Zuercher and R. Silbey, *J. Chem. Phys., 96* (1992) 6902; (f) R.W. Olson, J.S. Meth, C.D. Marshall, V.J. Newell and M.D. Fayer, *J. Chem. Phys., 92* (1990) 3323; (g) I.A. Walmsley and C.L. Tang, *J. Chem. Phys., 92* (1990) 1568; (h) Y.J. Yan and S.J. Mukamel, *Chem.*

Phys., 89 (1988) 5160; (i) J.A. Koningstein, *Chem. Phys. Lett., 146* (1988) 576; (j) B. Halperin, *Chem. Phys., 93* (1985) 39; (k) W.M. Gelbart, J.A. Beswick and G. Delgado-Barrio, *Can. J. Phys., 59* (1981) 1514; (l) D.A. Wiersma, *Adv. Chem. Phys., 47* (1981) 421; (m) J.M. Hayes, R.P. Stout and G.J. Small, *J. Chem. Phys., 74* (1981) 4266.

20 (a) R. Kubo, *Adv. Chem. Phys., 101* (1969); (b) L. Kador, *J. Chem. Phys., 95* (1991) 5574; (c) S.H. Simon, V. Dobrosavljević and R.M. Stratt, *J. Chem. Phys., 93* (1990) 2640; (d) R.I. Cukier and D.G. Nocera, *J. Chem. Phys., 97* (1992) 7371.

21 (a) W.B. Bosma, Y.J. Yan and S. Mukamel, *Phys. Rev. A, 42* (1990) 6920, and references therein; (b) M. Cho and G.R. Fleming, *J. Chem. Phys., 98* (1993) 2848; (c) J.C. Rasaiah and J. Zhu, *J. Chem. Phys., 98* (1993) 1213; (d) J. Zhu and J.C. Rasaiah, *J. Chem. Phys., 95* (1991) 3325; (e) J.M. Zaleski, C.K. Chang, G.E. Leroi, R.I. Cukier and D.G. Nocera, *J. Am. Chem. Soc., 114* (1992) 3564.

22 H. Graener, T. Lösch and A. Laubereau, *J. Chem. Phys., 93* (1990) 5365.

23 (a) R. Zwanzig, *J. Stat. Phys., 9* (1973) 215; (b) E. Pollack, *J. Chem. Phys., 85* (1986) 865; (c) M. Marchi, J.N. Gehlen, D. Chandler and M.D. Newton, *J. Am. Chem. Soc., 115* (1993) 4178; (d) A. Garg, J. Onuchic and V. Ambegaokar, *J. Chem. Phys., 83* (1985) 4491.

24 R. Islampour, R.G. Alden, G.Y.C. Wu and S.H. Lin, *J. Phys. Chem., 97* (1993) 6793.

25 A. Myers, personal communication, 1993.

26 (a) N. Kestner, J. Logan and J. Jortner, *J. Phys. Chem., 78* (1974) 2148; (b) J. Jortner, *J. Chem. Phys., 64* (1976) 4860; (c) R.R. Dogonadze, A.M. Kuznetsov and A.A. Chernenko, *Russ. Chem. Rev., 34* (1965) 759; (d) R.R. Dogonadze and Z. Urushadze, *J. Electroanal. Chem., 32* (1971) 235; (e) B.S. Brunschwig, J. Logan, M.D. Newton and N. Sutin, *J. Am. Chem. Soc., 102* (1980) 5798.

27 (a) N.S. Hush, *Prog. Inorg. Chem., 23* (1984) 3002; (b) R.S. Mulliken and W.B. Person, *Molecular Complexes*, Wiley, New York, 1969.

28 (a) R. de la Rosa, P.J. Chang, F. Salaymeh and J.C. Curtis, *Inorg. Chem., 24* (1985) 4229; (b) Y. Dong and J.T. Hupp, *Inorg. Chem., 31* (1992) 3170.

29 D. Oh and S.G. Boxer, *J. Am. Chem. Soc., 112* (1990) 8161.

30 M. Saheki, H. Yamada, H. Yoshioka and K. Nakatsu, *Acta Cryst. B, 32* (1976) 662.

31 (a) R.A. Marcus, *Discuss. Faraday Soc., 29* (1960) 21; (b) R.A. Marcus, *Ann. Rev. Phys. Chem., 15* (1964) 155; (c) R.A. Marcus, *J. Chem. Phys., 43* (1965) 2654; (d) R.A. Marcus, *J. Chem. Phys., 52* (1970) 2803.

32 M.R. Wasielewski, *Met. Ions Biol. Syst., 27* (1991) 361.

33 G.L. Closs and J.R. Miller, *Science, 240* (1988) 440.

34 W.H. Press, B.P. Flannery, S.A. Teukolsky and W.T. Vetterling, *Numerical Recipes* (FORTRAN *Version*), Cambridge University Press, Cambridge, 1989, p. 203.

35 (a) T. Kakitani and H. Kakitani, *Biochim. Biophys. Acta, 635* (1981) 498; (b) J. Ulstrup and J. Jortner, *J. Chem. Phys., 63* (1975) 4358.

36 (a) S.H. Lin, *J. Chem. Phys., 44* (1966) 3759); (b) R. Lagos and R.A. Friesner, *J. Chem. Phys., 81* (1984) 5899; (c) C.K. Chan and J.B. Page, *J. Chem. Phys., 79* (1983) 5234.

37 G.C. Walker, E. Åkesson, A.E. Johnson, N.E. Levinger and P.F. Barbara, *J. Phys. Chem., 96* (1992) 3728.

38 H. Sumi and R.A. Marcus, *J. Chem. Phys., 84* (1986) 4894.

39 J. Jortner and M. Bixon, *J. Chem. Phys., 88* (1988) 167.